Reviews in Mineralogy & Geochemistry
Vol. 86 pp. 217–240, 2021

Isotopic Traces of Atmospheric O_2 in Rocks, Minerals, and Melts

Andreas Pack

Georg-August-Universität Göttingen
Geowissenschaftliches Zentrum
Goldschmidtstraße 1
37077 Göttingen
Germany

apack@uni-goettingen.de

INTRODUCTION

In this chapter I review some of the knowledge about the oxygen isotope exchange between air O_2, rocks, minerals, melts, including some technical products. The rise of free atmospheric molecular oxygen since the great oxygenation event at the Archean–Proterozoic boundary 2.3 Ga ago (Farquhar et al. 2000; Luo et al. 2016) was one of the major events of the Earth environment. The triple oxygen isotope composition of atmospheric O_2 provides exciting insights into the Earth atmospheric composition and biosphere productivity (Bender et al. 1994; Luz et al. 1999, 2014; Luz and Barkan 2011; Young et al. 2014; Crockford et al. 2018). The triple isotope composition of O_2 of the past atmosphere can directly be obtained from ice cores (Blunier et al. 2002, 2012), but no such data are available for the time >1 Ma. Here, I review how one can get information about the isotope composition of atmospheric O_2 (especially $\Delta'^{17}O$) from rocks, minerals, and melts beyond the 1 Ma limit.

THE ISOTOPE COMPOSITION OF THE ATMOSPHERE

Modern air O_2

The modern atmosphere contains (by volume) 21% O_2 as the main oxygen-bearing component. With respect to molecular oxygen being the main oxygen-bearing component, this situation has been relatively stable at least during the Phanerozoic (for variations in O_2 partial pressures, see, e.g., Tappert et al. 2013). Before the rise of atmospheric O_2 2.3 Ga ago (Farquhar et al. 2000), CO_2 was likely the dominant oxygen-bearing species in the atmosphere (e.g., Catling and Zahnle 2020). In the present atmosphere, water vapor is the second most abundant oxygen-bearing species after O_2 roughly amounting ~ 1–2% at sea level and rapidly decreasing in concentration and mixing ratio with altitude. The upper troposphere and higher altitude atmospheric layers are very dry and contain only ≤5 ppmv water vapor (Leblanc et al. 2011). The third most abundant oxygen carrier in the modern atmosphere is CO_2, currently making up 0.04% and is increasing due to anthropogenic CO_2 emissions. Hence, for the upper atmosphere, 99.8% of oxygen is carried by O_2. Oxygen atoms are the dominant form above ~120 km At sea level, 96.4% of the oxygen is carried by O_2, 3.4% by vapor, and 0.2% by CO_2.

1529-6466/21/0086-0007$05.00 (print)
1943-2666/21/0086-0007$05.00 (online)
http://dx.doi.org/10.2138/rmg.2021.86.07

The isotopic compositions are expressed in form of the δ (McKinney et al. 1950) and $\Delta'^{17}O$ notations with:

$$\delta^{17}O = \left(\frac{\frac{^{17}O}{^{16}O_{Sample}}}{\frac{^{17}O}{^{16}O_{Reference}}} - 1 \right) \times 1000$$

$$\delta^{18}O = \left(\frac{\frac{^{18}O}{^{16}O_{Sample}}}{\frac{^{18}O}{^{16}O_{Reference}}} - 1 \right) \times 1000$$

$$\Delta'^{17}O = 1000 \times \ln\left(\frac{\delta^{17}O}{1000} + 1\right) - 0.528 \times \ln\left(\frac{\delta^{18}O}{1000} + 1\right)$$

One can debate whether the factor of 1000 is not already included in the ‰ notation. As it is referred to McKinney et al. (1950), I added the factor of 1000. Throughout this publication I use a $\Delta'^{17}O$ of San Carlos olivine of –0.052‰ as anchor point (average value of the studies of Pack et al. 2016; Sharp et al. 2016; Wostbrock et al. 2020) to ensure that $\delta^{17}O$ is reported relative to VSMOW scale (see also Miller and Pack 2021, this volume, and Sharp and Wostbrock 2021, this volume). Literature data were recalculated accordingly.

Early and first isotopic data of air O_2 have been reported from density measurements of waters by Dole (1936). He measured the isotope composition of air O_2 relative to the composition of Lake Michigan water ($\delta^{18}O = -5.9‰$). The "air" water sample was prepared by reacting atmospheric O_2 with H_2. In order to eliminate the effect of variable D/H ratios in the waters, Dole (1936) prepared two equivalent electrolysis cells and electrolyzed the "air" water and Lake Michigan water separately down to the same residual volume (40 ml). The generated O_2 from each water was purified and reacted with the same bottle of H_2 to produce water for density determination. The observed density difference between these two waters was only 6.0 ± 0.6 ppm, which transforms to a difference in atomic weights of oxygen in these waters of 0.000108 ± 0.00001 amu (Dole 1936). Casting this number into the now common $\delta^{18}O$ notation (McKinney et al. 1950), Dole (1936) determined that air O_2 has a $\delta^{18}O$ of 21.0 ± 1.5‰ relative to VSMOW. This remarkable number is, within uncertainty, identical to later and much more precise mass spectrometric measurements. Kroopnick and Craig (1972) measured the oxygen isotope composition of air O_2 by reacting the O_2 with hot (800–900°C) graphite leading to its conversion to CO_2. During the reaction, CO_2 was continuously separated by freezing it out with liquid nitrogen in order to shift the reaction quantitatively from CO towards CO_2. Because of isobaric interference of $^{13}C^{16}O_2$ with $^{12}C^{17}O^{16}O$, no $\delta^{17}O$ could be measured by these authors. The reported $\delta^{18}O$ was 23.5 ± 0.3‰. Thiemens and Meagher (1984) analyzed the $\delta^{17}O$ and $\delta^{18}O$ of air by cryogenetic separation of N_2 from O_2 in 13X molecular sieves and subsequent mass spectrometric analysis of the molecular oxygen. Nitrogen can be trapped at higher temperatures on molecular sieve than O_2 and Ar. Thiemens and Meagher (1984) obtained an average value of $\delta^{18}O = 23.43 \pm 0.07‰$ and $\Delta'^{17}O = -0.12 \pm 0.13‰$ (1σ SEM; $\Delta'^{17}O$ recalculated relative to a slope 0.528 reference line). The large uncertainty in $\Delta'^{17}O$ may be related to the fact that Ar was not separated from O_2 (which affects mass spectrometric sensitivity, see Barkan and Luz 2003) and/or that a dual collector instead of the now-common triple-collector mass spectrometer was used. Later, Thiemens et al. (1995) reported values for the atmospheric O_2 from high-altitude rocket launch experiments between 30 and 60 km altitude of $\delta^{18}O = 23.4 \pm 0.1‰$

and $\Delta'^{17}O = -0.4 \pm 0.1‰$. These air samples were treated as described in Thiemens and Meagher (1984). Barkan and Luz (2005) measured the composition of VSMOW water relative to the composition of their air reference (HLA, "Holy Land Air"). For the measurements, they applied a correction for the effect of Ar contamination in the samples. The O_2 of the VSMOW water was extracted using the CoF_3 fluorination method. They obtained a composition of their HLA of $\delta^{18}O = 23.88 \pm 0.02‰$ and $\Delta'^{17}O = -0.453 \pm 0.010‰$; again reported relative to 0.528 reference line. Later, Barkan and Luz (2011) revised their $\Delta'^{17}O$ for air O_2 to $-0.507 \pm 0.004‰$. Young et al. (2014) analyzed air O_2 and report a $\delta^{18}O$ of $23.533 \pm 0.007‰$ relative to VSMOW. The $\delta^{17}O$ of the reference gas tank was calibrated relative to O_2 extracted from San Carlos olivine with an assigned "$\Delta'^{17}O$" value of the San Carlos olivine of –0.004‰. Instead, the average $\Delta'^{17}O$ of San Carlos Olivine with both, $\delta^{17}O$ and $\delta^{18}O$ on VSMOW scale from Pack et al. (2016), Sharp et al. (2016), and Wostbrock et al. (2020), one obtains a value of –0.052‰.

Young et al. (2014) present an atmospheric mass balance model and analyzed the triple isotope composition of O_2 released from San Carlos olivine and O_2 extracted from air. Casting the $\delta^{17}O$ and $\Delta'^{17}O$ of Young et al. (2014) into a framework (slope 0.528 reference line) relative to San Carlos olivine with a $\Delta'^{17}O = -0.052‰$, a $\Delta'^{17}O$ of air O_2 of -0.422 ± 0.001 is obtained. Pack et al. (2017) reported a $\delta^{18}O$ of air of 24.15‰ and a $\Delta'^{17}O$ of $-0.424 \pm 0.008‰$ when recalculating their datum relative to San Carlos olivine at –0.052‰. Yeung et al. (2018) reported a composition of air O_2 ($\delta^{18}O$ = 23.6‰) with $\Delta'^{17}O$ relative to San Carlos olivine of $-0.421 \pm 0.004‰$. Including data reported relative to UWG2 garnet and assuming UWG2 garnet having a $\Delta'^{17}O$ = –0.061‰, gives $-0.423 \pm 0.002‰$ for Yeung et al. (2018). Wostbrock et al. (2020) also separated air O_2 from N_2 and Ar by means of low-*T* (–80°C) gas chromatography (Yeung et al. 2012; Young et al. 2014; Pack et al. 2017) and reported $\delta^{18}O = 24.05 \pm 0.11‰$ and $-0.441 \pm 0.012‰$. For this publication, we consider the composition of atmospheric O_2 to be $\delta^{18}O = 23.9 \pm 0.3‰$ and $\Delta'^{17}O = -0.432 \pm 0.015‰$ (1σ SD, weighted mean of Barkan and Luz 2005, Young et al. 2014, Pack et al. 2017, Yeung et al. 2018, and and Wostbrock et al. 2020; Fig. 1).

Including the datum of –0.507‰ by Barkan and Luz (2011) would pull the mean $\Delta'^{17}O$ value to –0.444‰. The reference gas used by Pack and Herwartz (2014) has been calibrated relative to VSMOW-SLAP calibrated tank O_2 relative to which the value of –0.507‰ has been measured. The reported $\Delta'^{17}O$ of San Carlos olivine in Pack and Herwartz (2014) then became –0.089‰

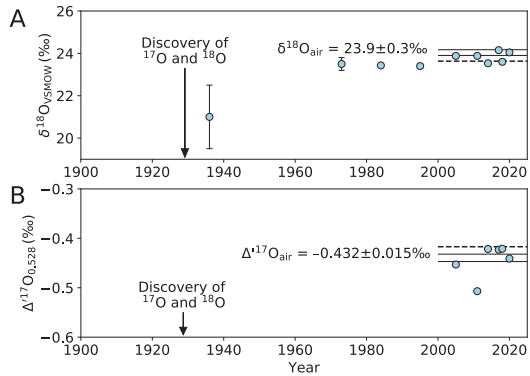

Figure 1. Plot of selected $\delta^{18}O$ (Dole 1936; Kroopnick and Craig 1972; Thiemens and Meagher 1984; Thiemens et al. 1995; Barkan and Luz 2005, 2011; Young et al. 2014; Pack et al. 2017; Yeung et al. 2018; Wostbrock et al. 2020) (**A**) and $\Delta'^{17}O$ (Barkan and Luz 2005, 2011; Young et al. 2014; Pack et al. 2017; Yeung et al. 2018; Wostbrock et al. 2020) (**B**) values of air O_2 vs. publication year. For calculation of the average composition of air O_2, we used published data by Barkan and Luz (2005), Young et al. (2014), Pack et al. (2017), Yeung et al. (2018), and Wostbrock et al. (2020). Giauque and Johnston (1929) first reported on ^{17}O and ^{18}O in air.

(recalculated relative to a slope 0.528 reference line), which is 0.051‰ lower than what later has been measured by direct comparison of O_2 from VSMOW and SLAP fluorination with O_2 from San Carlos olivine fluorination. Also, Sharp et al. (2016) and Wostbrock et al. (2020) obtained higher $\Delta'^{17}O$ values for San Carlos olivine than what was initially reported by Pack and Herwartz (2014). From this line of evidence, we favor excluding the −0.507‰ value and suggest a mean composition of air O_2 of –0.432 ± 0.015‰ (see also Sharp and Wostbrock 2021, this volume).

Notably, the studies on $\Delta'^{17}O$ of air O_2 show much larger discrepancies than can be explained by the respective reported analytical uncertainties only (see also Pack and Herwartz 2014). This shows that there are still systematic errors that need consideration.

Why is the reconstruction of the $\Delta'^{17}O$ of air O_2 from rocks interesting?

The isotope composition of rocks, minerals, and quenched melts is potentially preserved over millions to billions of years. Finding rocks, minerals, and glasses that have interacted with atmospheric oxygen may allow to reconstruct the past atmospheric isotope composition. This provides information about the atmospheric O_2 and CO_2 mixing ratios and global primary productivity (*GPP*, Luz et al. 1999; Young et al. 2014).

AIR–ROCK INTERACTION

Meteorite fusion crust

Meteorites are fragments of celestial bodies (Moon, planets, asteroids) that arrive on the Earth′s surface. Meteorites hit the Earth′s atmosphere with velocities in the range of 10 to 40 km s^{-1}. Friction with atmospheric molecules and atoms leads to heating of the meteoroid surfaces above their respective melting temperatures (Genge 2016). The interiors of larger meteorioids remain cool and only the outermost millimeter-thick layer is affected. Aerodynamic erosion of the melt layer leaves only a thin remaining fusion crust (Fig. 2).

Stony meteorite fusion crusts, however, are mixtures of the indigenous meteoritic material and melt exchanged oxygen or even equilibrated with air O_2 and other atmospheric gases like CO_2, but only when its partial pressure was higher than today (Payne et al. 2020). The indigenous meteorite material has very large variations in $\Delta'^{17}O$, which makes isolation of the atmospheric signature difficult.

In contrast, iron meteorites are composed of oxygen-free Fe, Ni alloy with minor sulfides. Oxides and silicates occur only in trace amounts (Buchwald 1977). The fusion crusts of iron meteorites are predominantly composed of magnetite (Fe_3O_4). The oxygen in that magnetite entirely sources from the atmosphere. Heinzinger et al. (1971) reported the first oxygen isotope analyses of iron meteorite crusts. Heinzinger et al. (1971) heated the oxidic fusion crust with graphite (t = 1350°C) under vacuum and formed CO and CO_2. The CO was quantitatively

Figure 2. Photography showing the 0.3 mm thin fusion crust of LL6 ordinary chondrite NWA 5882 (courtesy of Svend Buhl, https://www.meteorite-recon.com).

converted to CO_2 by glow discharge between Pt plates. The $\delta^{18}O$ was analyzed on the CO_2 by means of mass spectrometry. They observed $\delta^{18}O = 17.6 \pm 0.4‰$ for fusion crusts of unaltered iron meteorite falls (Braunau, IIAB; N′Goureyma, ungrouped; Trysa, IIIAB; Sikhote Alin, IIAB; classification from the Meteoritical Society Meteoritical Bulletin database). For the falls Braunau, Treysa, and Sikhote Alin, retardation heights of 15, 16, and 4.4 km were reported (Krinov et al. 1961), i.e., the fusion crust formed through oxidation by tropospheric O_2. The retardation height is the altitude, at which the strongest deceleration and heating occurs. Heinzinger et al. (1971) concluded that the observed –7‰ fractionation between the fusion crust and the atmosphere (using a value of $\delta^{18}O = 23.9‰$) is equilibrium fractionation between molten Fe-oxides and air O_2. They attributed lower $\delta^{18}O$ values of some fusion crusts to be the result of terrestrial weathering. Heinzinger et al. (1971) noted that I-type cosmic spherules, which they regarded as ablation products of iron meteorites and which are found in sediments, should record the $\delta^{18}O$ of the ancient atmosphere with an offset of –7‰. The $\delta^{18}O$ of the atmosphere, i.e., the $\delta^{18}O$ of molecular O_2 then would provide information about variations of the Dole effect on geological timescales.

More than a decade later, Clayton et al. (1986) analyzed the triple oxygen isotope composition of fusion crusts of six different iron meteorites, including some of those analyzed by Heinzinger et al. (1971) (Braunau, NGoureyma, Sikhote Alin, Treysa). The $\delta^{18}O$ values show a wide range from −10 to 15‰ with four out of the six meteorites clustering around 15‰ (Fig. 3), about ~2‰ lower than reported by Heinzinger et al. (1971). As did Heinzinger et al. (1971), Clayton et al. (1986) concluded that the 8‰ difference (using a value of 23.9‰ for air) between unaltered iron meteorite fusion crust and air O_2 reflects magnetite–O_2 equilibrium.

The triple isotope analyses of Clayton et al. (1986) allow one to test if the fusion-crust magnetite oxygen is of atmospheric origin and if equilibration occurred between magnetite and air O_2 (Fig. 3).

The low $\Delta'^{17}O$ of the fusion-crust magnetite that clusters around $\delta^{18}O = 15‰$ supports the hypothesis that the oxygen is at least partly of atmospheric origin. In contrast, the fusion crusts with $\delta^{18}O < 15‰$ have likely exchanged with meteoric water, removing much of the atmospheric O_2 signal. The lowest $\delta^{18}O$ is observed in fusion crusts of ALHA 76002, an Antarctic IIAB iron meteorite. The low $\delta^{18}O$ reflects exchange with Antarctic snow and ice.

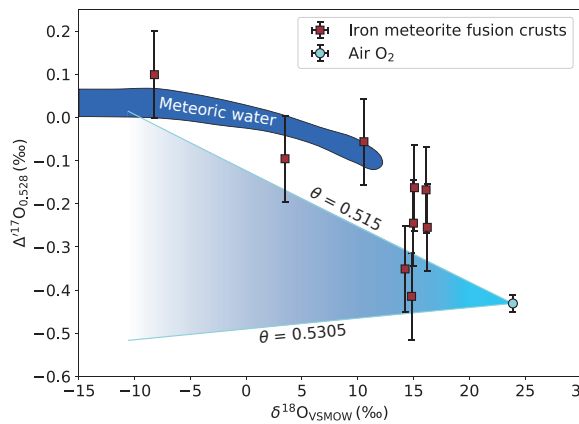

Figure 3. Plot of $\Delta'^{17}O$ vs. $\delta^{18}O$ of iron meteorite fusion crust (data from Clayton et al. 1986) and air O_2. ($\delta^{18}O = 23.9‰$, $\Delta'^{17}O = -0.431‰$). The composition of meteoric waters (including surface freshwater) is from a compilation of >1000 water analyses with data from Luz and Barkan (2010), Landais et al. (2008), Affolter et al. (2015), Li et al. (2015, 2017), Surma et al. (2015), Touzeau et al. (2016), Surma et al. (2018) Tian et al. (2018), and Tian and Wang (2019). The lowest $\delta^{18}O$ was observed for the fusion crust of Antarctic iron meteorite ALHA 76002.

The triple isotope data of Clayton et al. (1986), however, do not unequivocally support an equilibrium fractionation of 7–8‰ between magnetite fusion crust and air O_2 as suggested by Heinzinger et al. (1971) and Clayton et al. (1986). The high-temperature approximation for the equilibrium fractionation of oxygen is $\theta = 0.5305$ (Matsuhisa et al. 1978; Young et al. 2002). For high-temperature silicate and oxide mineral assemblages, Pack and Herwartz (2014) reported θ values in the range of 0.5281–0.5290. Instead, a kinetic isotope fractionation effect with a θ value around 0.515 is more compatible with the observations (Fig. 3). A short lifetime of the molten Fe oxide layer during the atmospheric entry is caused by intense aerodynamic erosion and likely prevents equilibration even at temperatures 1430 °C (minimum melting temperature in the magnetite–wüstite phase diagram; Laughlin and Hono 2015). Although not a high-temperature process, the chemisorption of oxygen on steel and copper is associated with a large kinetic fractionation of 26 and 61‰, respectively (Dole et al. 1954). Notably, the 61‰ for chemisorption of oxygen on Cu coincides with the fractionation assuming diffusion of O atoms and pure Graham′s law (Graham 1863) fractionation. The corresponding pure Graham′s law θ would be 0.515, which could explain the composition of iron meteorite fusion crust (Fig. 3). It should be emphasized here that the $\Delta'^{17}O$ data by Clayton et al. (1986) are not comparable in precision and accuracy as data obtained with modern mass spectrometers. Scale distortion effects (Yeung et al. 2018) may also have played a role. However, even if the fusion crust does not reflect isotope equilibrium with the atmosphere, triple oxygen isotope data of "fossil" iron meteorite fusion crust would still have the potential of providing information about the atmosphere. A 1‰ lower $\Delta'^{17}O$ of atmospheric O_2 would certainly be reflected in an about 1‰ lower $\Delta'^{17}O$ in the fusion crust. Data from unaltered, ancient "fossil" iron meteorite fusion crusts, however, have not yet been reported.

Cosmic spherules

During their atmospheric entry, meteoritic particles in the millimeter size range are heated and melted throughout to round spheres. These are termed cosmic spherules (Genge et al. 2008). A sub-group of these spherules are termed "I-type" cosmic spherules. These, often magnetic spherules were correctly identified as extraterrestrial in origin when they were first observed in deep-sea sediments collected during the research cruise of the HMS Challenger in the late 19th century. Heinzinger et al. (1971) suggested that these spherules are ablation products of iron meteorites. Although this view on their origin has not been supported by succeeding studies, Heinzinger et al. (1971) correctly noted "As these spherules are found in sediments of different geological ages, their oxygen isotope ratio can give information on the development of atmospheric oxygen." The oldest such cosmic spherules have been reported from Archean carbonates (Tomkins et al. 2016).

It is now established that cosmic I-type spherules form by oxidation of small Fe,Ni metal particles during atmospheric entry. Extraterrestrial Fe-Ni alloys with $5 \leq$ wt.% Ni ≤ 50 are not stable in the Earth atmosphere. Upon heating and melting during entry, the metal becomes oxidized. The I-type cosmic spherules are composed of Fe oxides (magnetite, wüstite) and, in some cases, residual Ni-rich metal. The oxides are Ni-poor compared to the original metal because Ni behaves more siderophilic than Fe during the oxidation. Clayton et al. (1986) reported the first triple isotope analyses of I-type cosmic spherules. Clayton et al. (1986) observed that I-type cosmic spherules (as do iron meteorite fusion crusts) roughly fall on a "terrestrial fractionation line", then defined as $\delta^{17}O = 0.52 \cdot \delta^{18}O$. Clayton et al. (1986) observed $40 \leq \delta^{18}O < 47$‰ for I-type spherules; a range much higher than what they observed for iron meteorite fusion crusts ($\delta^{18}O \approx 15$‰). From the fusion crust data and their supposed equilibrium with atmospheric O_2, Clayton et al. (1986) concluded that the Fe oxides in the small spherules equilibrated with the atmosphere with ~7–8‰ equilibrium fractionation. They hence concluded that the upper atmosphere in ~100 km altitude has a $\delta^{18}O$ in the range of 36‰, which is 12‰ higher than tropospheric O_2.

It was later reported by Davis et al. (1991) and Davis and Brownlee (1993) that Fe and Ni (Davis and Brownlee 1993) in I-type cosmic spherules are highly enriched in the heavy isotopes. The Fe isotope enrichment was reported to be 10–19‰ amu^{-1} and the Ni isotope enrichment was reported to be 4–32‰ amu^{-1}. Such extreme enrichment has neither been observed in terrestrial nor in any meteoritic metal. Davis and Brownlee (1993) concluded that between 74 and 94% evaporation led to the observed enrichment in Fe and Ni isotopes. Engrand et al. (2005) reported O, Fe, Ni, and Cr isotope compositions of I-type cosmic spherules from deep-sea sediments and confirmed strong isotope enrichments. Again, data were explained by mass fractionation during evaporation.

During mass fractionation, fractionation among the different isotope ratios is highly correlated so that mass-independent signals may be preserved. For oxygen this means that the $\Delta'^{17}O$ of air O_2 may still be preserved in I-type cosmic spherules although they have seen such massive evaporation. If so, Heinzinger et al. (1971) were right in their statement that I-type cosmic spherules can provide unique information about the atmospheric composition throughout the geologic history. In order to provide usable information about the ^{17}O anomaly of atmospheric O_2 it is necessary to analyze the $\Delta'^{17}O$ with an uncertainty $< \sim 0.1$‰, which is currently not achieved by ion microprobe measurements (Engrand et al. 2005).

Pack et al. (2017) reported measurements of the triple oxygen and iron isotope composition of Antarctic I-type spherules. They used laser fluorination in combination with gas source mass spectrometry in continuous-flow mode and analyzed a small set of large I-type cosmic spherules collected in Antarctica. They reported $\delta^{18}O$ values between 36 and 42‰, well within the ranges reported by Clayton et al. (1986) and Engrand et al. (2005). The aim of this study was to test the hypothesis that the Earth′s atmosphere is isotopically homogenous up to ~ 100 km altitude. In order to quantify the degree of evaporation, Pack et al. (2017) measured the Fe isotope composition of the spheres. In contrast to oxygen, there is no Fe in the atmosphere and exchange with the atmosphere does not influence the Fe isotope composition. Therefore, $\delta^{56}Fe$ was regarded as a solid constraint for the degree of evaporation. Wang et al. (1994) conducted evaporation experiments for FeO melts. They observed that the $\delta^{18}O$ and $\delta^{56}Fe$ both increase with increasing degree of evaporation. From the experiments of Wang et al. (1994), Pack et al. (2017) calculated an empirical relation for the Fe and O isotope fractionation during evaporation with $\ln(\delta^{18}O + 1) = 1.18 \cdot \ln(\delta^{56}Fe)$. This relation allowed a reconstruction of the pre-evaporation composition of the I-type spherules, i.e., the composition of the spherules after melting and oxidation, but before evaporation. Spherules with such a composition, of course, do not exist during atmospheric entry because melting and oxidation and evaporation probably occur all at the same time. For the modeling, however, it is useful to disentangle the two processes: fractionation during oxidation and during evaporation. The suggested pre-evaporation oxygen isotope compositions of the studied I-type spherules were in the range $2 \leq \delta^{18}O \leq 14$‰, i.e. considerably lighter than air O_2. The discrepancy between air O_2 ($\delta^{18}O = 24$‰) and pre-evaporative compositions of the spherules ($\delta^{18}O \approx 8$‰) is on the same order as that observed in iron meteorite fusion crusts (Fig. 3), where evaporation does not play a role. This fractionation was attributed to kinetics during metal oxidation.

Fractionation of isotopes during evaporation is dominated by kinetic fractionation with an associated θ that is generally "low". This is true for both Fe and O. Although analytical precision was likely lower than what nowadays can be achieved, the experiments by Wang et al. (1994), indeed, show that during evaporation, the associated θ for triple oxygen is as low as 0.510. It is interesting to note that also the θ for Fe is low, i.e., variations in θ can not only be observed for a light element like oxygen, but also for heavy elements. Apart from the evaporation, Pack et al. (2017) also considered kinetic fractionation during oxidation of the metal. As mentioned above, very large isotope effects were observed by Dole et al. (1954) for the oxidation of steel (–26‰ in $^{18}O/^{16}O$) and oxidation of copper (–61‰ in $^{18}O/^{16}O$). The high-*T* oxidation experiments by Pack et al. (2017) were associated with a –4‰ fractionation in $\delta^{18}O$. Along with the iron meteorite fusion rusts as natural experiments, an associated $\theta_{oxidation} = 0.506$ was suggested.

In conclusion, Pack et al. (2017) demonstrated that the isotope composition of the Earth′s atmosphere is homogenous with respect to $\Delta'^{17}O$ up to ~100 km and that I-type cosmic spherules are suitable tracer for the $\Delta'^{17}O$ of the atmosphere. because $\Delta'^{17}O$ of atmospheric molecular O_2 is function of *GPP* and atmospheric CO_2 mixing ratios, fossil cosmic spherules are very interesting proxies.

From air to sulfates and beyond

The triple isotope composition of sedimentary sulfates is reviewed in detail by Bao (2015), Bao et al. (2016), and Cao and Bao (2021, this volume) and only a short overview is given here. It has been observed that sedimentary sulfates can carry a distinctly negative $\Delta'^{17}O$ when compared to other sedimentary minerals (Bao et al. 2008). The only component known on Earth that carries a negative anomaly in $\Delta'^{17}O$ is atmospheric O_2, which counter balances the positive anomalies of O_3 and stratospheric CO_2. Bao et al. (2008) suggested that the negative anomaly down to –0.7‰ that they have observed in Neoproterozoic barites is inherited by the sulfate from the process of subaerial sulfide (e.g., pyrite) oxidation in an overall reaction:

$$2\ FeS_2 + 7.5\ O_2 + 4\ H_2O \rightarrow Fe_2O_3 + 4\ H_2SO_4$$

As such, sedimentary sulfate can be used to obtain information on the $\Delta'^{17}O$ of atmospheric O_2. This information provides insights into the *GPP* and p_{CO_2} (Bender et al. 1994; Luz et al. 1999; Blunier et al. 2002; Young et al. 2014). The uncertainty in this approach is dominated by the uncertainly of the portion of oxygen sourcing from O_2, (see Kohl and Bao 2011) but also depends on the assumed *GPP* and the stratosphere–troposphere exchange mass flux (Cao and Bao 2013; Graham et al. 2019). The high p_{CO_2} estimates of up to 20,000 ppmv by Bao et al. (2008) are based on the assumption of the same *GPP* in the Neoproterozoic as today. A dynamic view of the evolution of atmospheric p_{CO_2}, p_{O_2}, and *GPP* in a post-Snowball Earth meltdown world can be found in Cao and Bao (2013). Crockford et al. (2018) also reported $\Delta'^{17}O$ of Proterozoic sulfates with minimum $\Delta'^{17}O$ of –0.88‰. They concluded that the *GPP* was only 6–41% of modern *GPP*, depending on the assumed atmospheric O_2 mixing ratio (0.02–2 vol.%) and p_{CO_2} (540–8100 ppmv).

Peters et al. (2020) investigated the triple oxygen isotope composition of magnetite from iron deposits in Iran by means of high-precision laser fluorination. They observed that magnetite from the Yazd iron oxide–apatite deposit shows a significant negative anomaly down to –0.2‰, which Peters et al. (2020) related to the incorporation of oxygen from older sulfate from late Proterozoic, early Cambrian evaporite rocks reported by Crockford et al. (2018) from that region. These evaporites, in turn, had obtained a negative anomaly inherited from subaerial sulfide oxidation as originally suggested by Bao et al. (2008). By their triple oxygen isotope data, Peters et al. (2020) could exclude that the magnetite from the Yazd deposit last equilibrated with "normal" magmatic fluids.

The study of Peters et al. (2020) shows that $\Delta'^{17}O$ anomalies can be a robust tracer for the pathway of oxygen in complex geologic processes. On its pathway from air through pyrite oxidation, sulfate dissolution, sulfate reduction, fluid mobilization and participation in magnetite precipitation, much of the $\Delta'^{17}O$ has been diluted with "normal" oxygen but some atmospheric signature is preserved. The observed $\Delta'^{17}O$ can therefore only be regarded as a maximum value during the time of evaporite precipitation with limited information on $GPP \cdot p_{CO_2}$. Surely, direct analyses of the sulfate as reported by Crockford et al. (2018) from the same region provide more information. Nevertheless, the study by Peters et al. (2020) is yet another trace of anomalous atmospheric oxygen in rocks and can be applied in cases where no evaporite is preserved and/or accessible.The magnetite $\Delta'^{17}O$ provides information about the minimum anomaly in ^{17}O and hence provides a minimum $GPP \cdot p_{CO_2}$ number. Caution must be exercised when dealing with sulfate $\Delta'^{17}O$ that are within ±0.25‰, as various mass-dependent processes can also impart small, yet variable ^{17}O anomalies for sulfate (Cao and Bao 2021, this volume).

Deep sea manganese nodules

Large portions of the deep oceans floor are covered by small, centimeter-sized ferromanganese nodules. These nodules formed by oxidation of dissolved Mn^{2+} and precipitation of Mn-IV-oxides. The oxidation of Mn^{2+} requires a strong oxidizer, which is dissolved O_2. The isotope composition of seawater dissolved O_2 is closely linked to the composition of air O_2, which makes ferromanganese nodules a potential archive for the isotope composition of tropospheric O_2, especially the $\Delta'^{17}O$.

As in the case of sedimentary sulfate or cosmic spherules, oxidation of Mn^{2+} by O_2 involves mass-transfer of O_2 into the resultant Mn-IV-oxides ("MnO_2", manganates). Unlike in the process of oxidation of ferric to ferrous iron in aqueous solution, the isotope signature of O_2 is partially preserved in the MnO_2 phases. Mandernack et al. (1995) demonstrated that experimentally precipitated manganate (abiological and biological) contains 32–50% oxygen from dissolved O_2 with the remaining oxygen in the manganate sourcing from H_2O. This is in the same range as suggested for the pyrite-derived sulfate (8–15%, Balci et al. 2007; 0–60%, Kohl and Bao 2011). The isotope fractionation between O_2 and manganate, however, was measured to vary between ~ 0 and –22, which complicates the interpretation of ferromanganese nodule oxygen isotope data. The fractionation between H_2O and manganate precipitate was measured to vary between –5 and 1‰ (Mandernack et al. 1995), which is similar to the fractionation between H_2O and iron oxides. For the interpretation of ferromanganese nodule data, it also has to be considered that they are a mixture of manganate, authigenic silicates, and Fe oxides. The authigenic silicates and the Fe oxides are not expected to carry the anomalous signature of atmospheric O_2. A further aspect that needs consideration when using manganese nodules as a paleoatmospheric-archive is that the isotope composition of seawater dissolved O_2, i.e., the Mn^{2+} oxidizer, is not identical to that of tropospheric O_2, the eventual quantity of interest.

The equilibrium fractionation between dissolved O_2 in water and air at 25°C is $1000 \cdot \ln(\alpha_{O_2,diss.-air}) = 0.7‰$ (Benson and Krause 1984; Li et al. 2019), i.e., the oxygen dissolved in the ocean surface layer in immediate contact with air has $\delta^{18}O \approx 25‰$. The corresponding $\Delta'^{17}O$ is close to the value for air O_2, i.e., –0.432‰. This oxygen is mixed with photosynthetic O_2, which has an isotope composition close to that of seawater. Photosynthesis in the photic zone produces O_2 with $\delta^{18}O \approx \Delta'^{17}O \approx 0‰$. Mixing of anomalous air O_2 with such O_2 leads to an increase of dissolved O_2 $\Delta'^{17}O$ with increasing O_2 concentration (e.g., Luz and Barkan 2000, 2009, their Fig. 2). At depths of a few hundred meters, respiration consumes dissolved O_2 and enriches the remaining dissolved O_2 in ^{17}O and ^{18}O relative to ^{16}O (Dole effect, Dole et al. 1954). In this oxygen minimum zone, Kroopnick and Craig (1976) measured $\delta^{18}O$ values for the dissolved O_2 as high as 38‰. Respiration is a kinetic process and is accompanied by a $\theta_{resp.}$ in the range of 0.518, i.e., respiration leads to a decrease in $\Delta'^{17}O$ with increasing $\delta^{18}O$ when reporting $\Delta'^{17}O$ relative to a reference line with slope 0.528. The precise value for $\theta_{resp.}$ depends on a variety of factors and it is referred to recent works by Stolper et al. (2018) or Ash et al. (2020) for details. Only a small number of studies report the triple isotope composition of O_2 dissolved in abyssal regions of world oceans (here, we consider data from depths >1000 m). Recasting the data reported by Yeung et al. in the online data repository at https://www.bco-dmo.org/dataset/753594 as of 2020 with $\delta^{17}O$ and $\delta^{18}O$ on VSMOW scale and $\Delta'^{17}O$ relative to a slope −0.528 reference line gives deep-Pacific data with $32 \le \delta^{18}O \le 40‰$ and $\Delta'^{17}O$ falling along a slope ~ 0.518 trend (Fig. 4). This trend coincides with the respirators fractionation trend, but is a result of complex relations between fractionation and mixture processes (Hendricks et al. 2005; Nicholson et al. 2014). The fan-shape of the area covered by data (Fig. 4) indicates that mixing between photosynthetic O_2 and anomalous air O_2.

Recently, Sharp et al. (2018) and Sutherland et al. (2020) reported the first high-precision triple oxygen isotope data of ferromanganese nodules from the ocean floor. Sutherland et al. (2020) clearly identified anomalous oxygen in their set of ferromanganese nodules (Fig. 4). Their interpretation, in line with experimental work of Mandernack et al. (1995), is that these marine Mn-IV-oxides preserved the anomaly of dissolved O_2 and hence are potential archives for dissolved O_2 that had exchanged with atmospheric O_2.

Here I discuss the interpretation of the Sutherland et al. (2020) data in terms of hypothetical Mn oxide endmembers. Mn oxides that form in equilibrium with seawater would have a composition as marked "Mn oxide I" in (Fig. 4). If Mn oxides formed by oxidation of deep sea dissolved O_2 only, their composition is expected to plot somewhere between the composition of the dissolved O_2 ("Mn oxide II"; no fractionation between O_2 and Mn oxide) and a composition marked "Mn oxide III" with 20‰ kinetic fractionation between O_2 and Mn oxide (Mandernack et al. 1995). A $\theta_{kinetic}$ of 0.515 has been assumed (Sutherland et al. 2020) and we adopt this value here. For details on mechanisms of O_2 binding and O_2 reduction I refer the interested reader to, e.g., Ash et al. (2020). Assuming that the Mn is oxidized in ocean layers that were

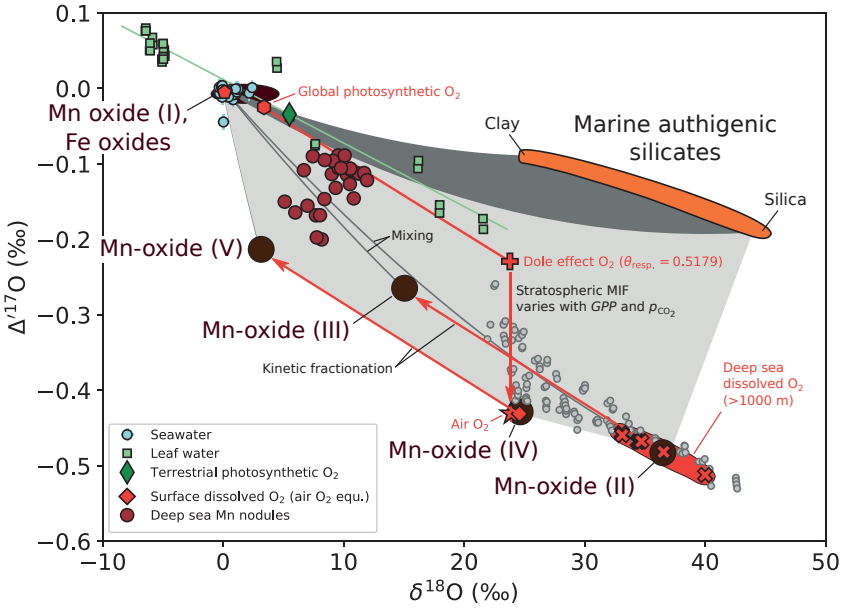

Figure 4. Plot of $\Delta'^{17}O$ vs. $\delta^{18}O$ illustrating the oxygen pathways and sources of deep-sea ferromanganese nodules (**brown filled circles**, Sutherland et al. 2020). I assume that photosynthetic oxygen (**red filled hexagon**) is a mixture of marine (**red filled pentagon**) and terrestrial (**green filled diamond**; average composition of leaf water) photosynthesis. The seawater composition (**light blue filled circles**) is from Barkan and Luz (2011). The marine authigenic clay composition is from Sengupta and Pack (2018). The silica composition is from Sharp et al. (2016). The **dark grey filled area** outlines oxygen mixing between authigenic minerals (clay, silica) and seawater. The dissolved O_2 isotope data (**light gray filled circles**, >1000 m: **red filled crosses**) are taken from Yeung et al.'s dataset https://www.bco-dmo.org/dataset/753594 as of 2020. "Mn oxides I" outlines the composition of Mn and Fe oxides in equilibrium with seawater. "Mn oxides II" have acquired the entire oxygen from deep-sea dissolved O_2 without fractionation (Mandernack et al. 1995), whereas "Mn oxide IV" would have acquired the oxygen from air equilibrated dissolved O_2. "Mn oxide III and V" would have formed from the respective dissolved O_2 under participation of a 20‰ kinetic isotope fractionation (Mandernack et al. 1995). The **light gray shaded area** outlines the possible field for bulk ferromanganese nodules.

well-mixed with the atmosphere, and no fractionation would occur during the oxidation, Mn oxide would have a composition identical to that of dissolved and air equilibrated O_2 ("Mn oxide IV"). This composition has been considered as one endmember by (Sutherland et al. 2020). If 20‰ fractionation is associated with the oxidation of Mn (Mandernack et al. 1995), one would get a Mn oxide endmember with a composition labeled "Mn oxide V". This is the second endmember considered by Sutherland et al. (2020). Any of these pure endmembers are likely to exist. The experiments by Mandernack et al. (1995) show that during the oxidation, also equilibration with the surrounding water plays a role and only ~40% of the oxygen in the Mn oxides sources from O_2. This means that the Mn oxides in ferromanganese crusts are expected to have compositions on the mixing trends between "Mn oxides II–V" and the water equilibrated "Mn oxide I". Because the ferromanaganese nodules form in the deep sea, a mixture between "Mn oxide II" and "Mn oxide III" should be considered rather than "Mn oxide IV" and "Mn oxide V". Bulk ferromanganese nodules are mixtures of Mn and Fe oxides, and silicates. The Fe oxides will have a composition close to that of seawater. Following the suggestion by Sutherland et al. (2020), the silicate fraction can be approximated by a mixture of silica (Sharp et al. 2016) and clay (from Sengupta and Pack 2018; orange filled region in Fig. 4).

The composition of bulk ferromanganese nodules is expected to fall in the light gray shaded area, which is, indeed, the case (Fig. 4). Because of their deep-sea formation and considering 40% O_2 in the Mn oxides, the data by Sutherland et al. (2020) can be explained by "Mn oxide III" as one endmember, mixed with seawater-equilibrated Fe and Mn oxides and various portions of silicates. In such a model, those deep-sea ferromanganese nodules with $\Delta'^{17}O$ below the "Mn oxide II,III"–"Mn oxide I, Fe oxide" mixing trend would be explained by a lower $\Delta'^{17}O$ of atmospheric O_2. A lower $\Delta'^{17}O$ of atmospheric O_2 could be due to elevated p_{CO_2} and/or decreased *GPP* (Bender et al. 1994; Luz et al. 1999; Young et al. 2014). As a quantitative paleo-CO_2 and paleo-*GPP* proxy, more data are required to better understand the particular fractionation processes during the crust formation. Nevertheless, the deep-sea ferromanganese nodules are an interesting target for future triple oxygen isotope studies.

Tektites

Air melt exchange. Urey (1955) discussed the origin of tektites and concluded that they are of extraterrestrial origin. He based his argument on the observation of tektite liquidus temperatures that are beyond temperatures known from magmatic processes and their (intergroup) chemical homogeneity that is unrelated to the local rock chemistry. He also noted that tektite occurrences are unrelated to the spatial distribution of terrestrial volcanism. Based on their distribution on Earth, Urey (1955) speculated that tektites may have arrived from the Moon. The chemical composition of tektites, however, is very similar to that of the Earth′s crust and makes a lunar origin less likely. Two decades earlier, Spencer (1933) had put forward the now-established idea that tektites formed during melting end ejection of target rock during a meteorite impact. He based his suggestion on the occurrence of tektites in the vicinity of impact craters and on the chemical similarity of tektites and the Earth surface material. A review on the origin of tektites on basis of geochemistry is given by Koeberl (1988, 1994).

The first oxygen isotope data of tektites was published by Silverman (1951). He analyzed tektites from the Phillippines, which belong to the Australasian strew field, and from Bohemia (moldavites), which were ejected from the Ries crater in Southern Germany ~15 Ma ago. For both glasses, Silverman (1951) measured $\delta^{18}O = 10.4‰$. He noted that their composition is different from stony meteorites, but similar to terrestrial sedimentary rocks. He leaves the reader with the options that tektites are either of terrestrial origin or of extraterrestrial origin and that similar sedimentary processes that enrich rocks in ^{18}O operate on other bodies of the Solar System. Taylor and Epstein (1962) analyzed a wider range of tektites and found $\delta^{18}O$ in a narrow range between 9.6 and 10.4‰. They noted that the oxygen-isotope composition resembles that

of felsic igneous rocks, whereas their chemistry rather agrees with that of sedimentary rocks. Sedimentary rocks, however, typically have $\delta^{18}O > 10‰$. In conclusion, Taylor and Epstein (1962) suggested that tektites were of extraterrestrial origin. The total range of published tektite data is $7 \le \delta^{18}O \le 15‰$ (see Zák et al. 2019, and references therein), i.e., covering the range typical of sedimentary rocks.

The first triple oxygen isotope data for tektites were published by Clayton and Mayeda (1996). They reported data for 14 tektites of different origin. Their $\delta^{18}O$ values range between 8.6 and 10.3‰, typical for continental surface rocks (e.g., Bindeman 2021, this volume). All tektite data are in the $\delta^{18}O$ range typical for sedimentary rocks and are by <10‰ lighter than air O_2. If one assumes that the equilibrium fractionation at high temperatures is small, this suggests little exchange between atmospheric O_2 and tektites. This conclusion is supported by the $\Delta'^{17}O$ values of Clayton and Mayeda (1996). Casting their data into the $\lambda_{RL} = 0.528$ framework, their average $\Delta'^{17}O$ is –0.08‰ with a 1σ standard deviation of the mean 0.05‰ (Fig. 5). This puts the tektites well in the field of terrestrial rocks (Sharp et al. 2018; Bindeman 2021, this volume), but is much higher than the –0.432‰ of air O_2. More triple isotope data of tektites were published by Zák et al. (2019) on tektites from the Australasian strew field (Fig. 5). Their $\delta^{18}O$ values range from 8.7 to 11.6‰, a typical range for sedimentary rocks. The reported $\Delta'^{17}O$ values (cast into $\lambda_{RL} = 0.528$ notation) range from –0.07 to –0.04 with an average of –0.055 and a standard deviation of 0.010‰. As in case of the data by Clayton and Mayeda (1996), the new data fall well within the range typical of terrestrial rocks. No indication for exchange with air O_2 is observed in the dataset by Zák et al. (2019).

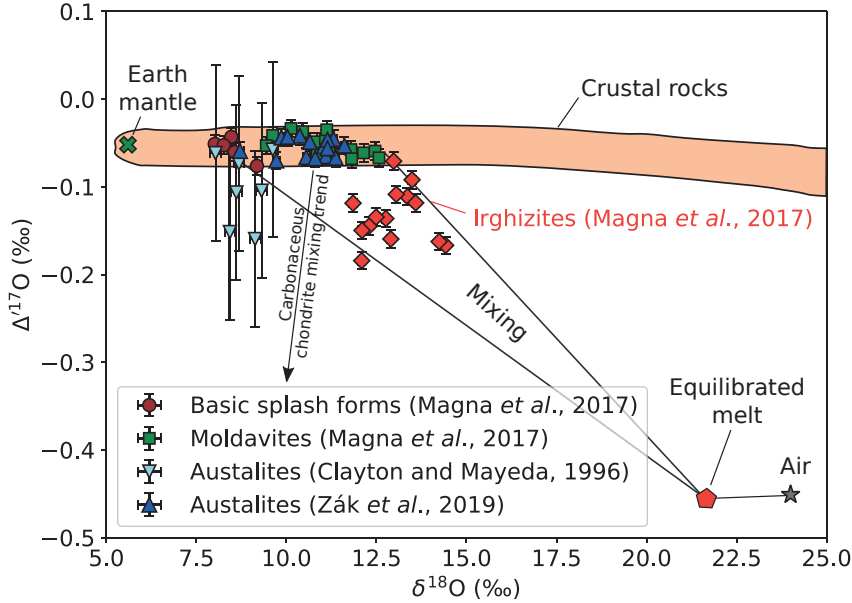

Figure 5. Plot of $\Delta'^{17}O$ vs. $\delta^{18}O$ of triple oxygen isotope data of tektites (data are from Clayton and Mayeda 1996, Magna et al. 2017, and Zák et al. 2019). Most tektites follow a narrow trend with $\Delta'^{17}O$ close to the composition of the Earth mantle with $\delta^{18}O$ typical of felsic igneous and sedimentary rocks (e.g., Pack and Herwartz 2014; Bindeman et al. 2018, 2019; Bindeman 2021, this volume). For the Clayton and Mayeda (1996) data an uncertainty in $\Delta'^{17}O$ of ± 0.1‰ is assumed. The more recent data have an uncertainty of only 0.01‰ and demonstrate the progress made in the analytical protocols for triple oxygen isotope analyses. The irghizites follow a mixing trend between target material and silicate melt that equilibrated with air O_2 (**red filled pentagon**; see explanation below).

Magna et al. (2017) published triple oxygen isotope data on Moldavites and glasses from the ~ 1 Ma old Zhamanshin impact crater in Kazahstan (48°24′N 60°58′E, see also Florenski 1977, Bouşka et al. 1981, and Koeberl and Fredriksson 1986; Fig. 5). The $\delta^{18}O$ values of the Moldavites and the basic splash forms from the Zhamanshin impact site (excluding the irghizites) range from 7 to 12‰ and fall within the range of tektites from other localities. The $\Delta'^{17}O$ values for moldavites, i.e., the ejecta from the ~ 15 Ma old Ries impact structure (48°53′N, 10°32′E), and the basic splash forms from the Zhamanshin impact range from –0.068 to –0.033‰ and are indistinguishable from sedimentary rocks with similar $\delta^{18}O$ (Sharp et al. 2018; Bindeman 2021, this volume).

Only the felsic irghizites ejected from the Zhamanshin crater plot outside the field typical for sedimentary and igneous rocks and show distinct lower $\Delta'^{17}O$ values (Fig. 5, red filled diamonds). For these impact glasses, lower $\Delta'^{17}O$ could either come from mixing of target rock with a carbonaceous chondrite impactor or from exchange with low $\Delta'^{17}O$ atmospheric oxygen. Magna et al. (2017) excluded that the low $\Delta'^{17}O$ is due to admixing of a carbonaceous chondrite component. If so, a steep vertical trend is expected (Fig. 5). Instead, the irghizites follow a trend that can broadly be explained by exchange of the melt with atmospheric oxygen. Magna et al. (2017) assumed that the fractionation between silicate melt and O_2 is negligible at the high temperatures of the impact. The age of the Zhamanshin crater is ~ 1 Ma. At this time, the $\Delta'^{17}O$ of the atmospheric O_2 was similar to today, i.e. ~ –0.4‰. It is noted here that glacial–interglacial variations in atmospheric $\Delta'^{17}O$ amount for as much as 0.06‰ in $\Delta'^{17}O$ (Blunier et al. 2012).

Why do the irghizites appear to have exchanged with the atmosphere whereas the Zhamanshin basic splash forms, Moldavites and Australites do not? The sizes of the Zhamanshin crater (source of the irghizites) and the Ries crater (source of the Moldavites) are both 15 km, so it is not likely the intensity of the impact that makes the difference. Irghizites are found close to the crater, whereas Moldavites and Australites have been transported hundreds to thousands of kilometers away from the impact site. For these proximal tektites, Mizera et al. (2012) suggested longer heating times compared to the distal tektites. Another feature that distinguishes the irghizites from other, distal tektites is the "effective" size. The irghizites are often composed of agglomerates of small former melt spherules (Mizera et al. 2012), which reduces the "effective" size, i.e., the size relevant for estimating the exchange rate with the ambient atmosphere. The surface/volume ratio of these spherules is orders of magnitude larger than for the monolithic distal tektites. Both prolonged heating times and smaller "effective" size of the irghizites compared to Moldavites and Australites could explain why the irghizites exchanged oxygen with the atmosphere, whereas the latter two did not.

However, are the short heating times in the range of a few minutes at maximum sufficient to exchange ~ 20% oxygen with the atmosphere as has been concluded by Magna et al. (2017)? In order to test what heating times are required to exchange oxygen between O_2 and silicate melts, we conducted experiments in our laboratory. Silicate samples (49 wt.% SiO_2, 23 wt.% CaO, 11 wt.% Al_2O_3, 17 wt.% MgO, $T_{liquidus} \approx 1350$ °C, phase diagram from Winter 2001, p. 106) were melted for different times (5 s–50 min) in a Gero vertical gas mixing furnace using the Pt-loop technique (Donaldson et al. 1975). Iron was avoided in order to reduce complexity due to redox-related mass transfer between the melt and the atmosphere and the melt and the Pt loop. The diameter of the sample loops was roughly 2–3 mm. Temperatures were 1350 °C and 1500 °C, both above the liquidus of the chosen composition. The furnace atmosphere was air. The oxygen isotope composition of the samples was analyzed by laser fluorination in combination with gas-source mass spectrometry. At time of the project, problems with the source controller board prevented use of the Thermo MAT253 mass spectrometer and a gas chromatograph. Therefore, all analyses on the starting materials and run products were conducted offline, i.e., by transferring the samples in glass vials filled with 5Å molecular sieve to a Finnigan DeltaPlus mass spectrometer and without gas chromatographic purification. Therefore, the uncertainty in $\Delta'^{17}O$ was ± 0.03‰. San Carlos olivine was used as standard. The results are listed in (Table 1) and illustrated in (Fig. 6).

The data demonstrate that 20% exchange between silicate melt and atmospheric O_2 occurs within < 1 min. It is therefore conceivable that the spherules forming the irghizites have exchanged with the atmosphere during their minutes-long residence time in the hot impact plume (Shuvalov and Dypvik 2013). A second result of the experiments is that the equilibrium fractionation between air O_2 and silicate melt at 1350 and 1500 °C is still about −2.5‰ (Fig. 6). Although associated with a large uncertainty, an associated high-T θ of 0.5290–0.5305 is compatible with the observation. Also, the data suggest that the silicate analyses and the analyses of air O_2 are on the same scale for $\delta^{17}O$. High-T equilibration of silicate melt with excess air O_2 using the air data by Pack et al. (2017) or Wostbrock et al. (2020) could be a means of calibrating the $\Delta'^{17}O$ of laboratory reference gases relative to the VSMOW.

The data by Magna et al. (2017) show that tektites can have ~ 20% exchange with atmospheric oxygen, if the individual melt droplets are in the millimeter size range. In order to use fossil tektites as a proxy for $p_{CO_2} \cdot GPP$, it is necessary to extrapolate the tektite data toward the locus of equilibrated melt at a $\delta^{18}O$ of about 21.5‰ in order to account for the equilibrium fractionation between O_2 and silica melt. The use of tektites as a paleo-$CO_2 \cdot GPP$ proxy, however, requires that the data plot along a narrow trend instead of showing large, uncorrelated variations in $\delta^{18}O$ and $\Delta'^{17}O$ as observed by Magna et al. (2017) (Fig. 5).

The experimental data (Fig. 6) suggest that at 1350–1500 °C exchange occurs within tens of seconds to minutes, timescales that can be realized in impact plumes. Temperature in the impact plume could well have been higher than the experimental temperatures (Macris et al. 2018), which would further accelerate the exchange. It is therefore conceivable that detailed analyses of, e.g., only outer layers of tektites could show more exchange or even equilibration and thus would make a suitable proxy for the $\Delta'^{17}O$ millions of years back from now.

Table 1. List of the experimental samples and the corresponding oxygen isotope data (Stübler 2017). The $\Delta'^{17}O$ is reported relative to a slope − 0.528 reference line.

Sample	**Comment**	$\delta^{17}O$	$\delta^{18}O$	$\Delta'^{17}O$
CSS	Starting material	3.78	7.36	−0.10
CS5−1350	t = 5 s, T = 1350 °C	5.06	9.97	−0.19
CS10−1350	t = 10 s, T = 1350 °C	6.1	11.96	−0.20
CS40−1350	t = 40 s, T = 1350 °C	6.42	12.77	−0.30
CS60−1350	t = 60 s, T = 1350 °C	6.04	11.9	−0.23
CS160−1350	t = 160 s, T = 1350 °C	7.57	14.87	−0.26
CS640−1350	t = 640 s, T = 1350 °C	10.89	21.58	−0.44
CS1280−1350	t = 1280 s, T = 1350 °C	10.68	21.21	−0.46
CS2560−1350	t = 2560 s, T = 1350 °C	10.54	21	−0.49
CS2997−1350	t = 2997 s, T = 1350 °C	10.5	20.78	−0.42
CS10−1500	t = 10 s, T = 1500 °C	7.38	14.55	−0.27
CS15−1500	t = 15 s, T = 1500 °C	8.4	16.62	−0.34
CS35−1500	t = 35 s, T = 1500 °C	9.87	19.59	−0.42
CS105−1500	t = 105 s, T = 1500 °C	10.82	21.43	−0.43
CS240−1500	t = 240 s, T = 1500 °C	10.85	21.37	−0.37
CS960−1500	t = 960 s, T = 1500 °C	11	21.75	−0.42
San Carlos olivine	average (N = 7)	2.69	5.19	−0.05

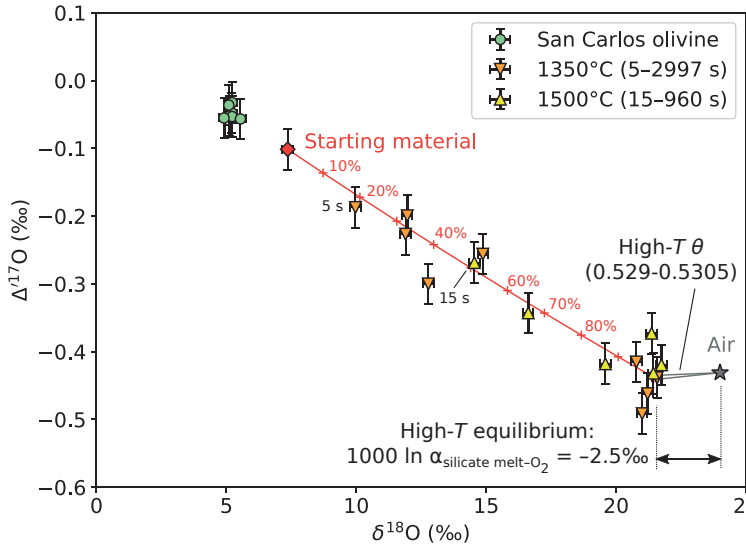

Figure 6. Plot of $\Delta'^{17}O$ vs. $\delta^{18}O$ of silicate melt (**red filled diamond**) and air (**gray filled star**) equilibrated for different times at 1350°C (**orange**) and 1500°C (**yellow**). At prolonged equilibration times, silicate melt and air O_2 come into equilibrium with a fractionation of ~ –2.5‰. The study was conducted within a BSc thesis project by Christian Stübler in 2017. The data are listed in (Table 1).

Air inclusions in tektite glasses

Tektites may preserve information about the atmosphere at time of their formation other than by having isotopically exchanged. Instead, bubbles of air could potentially be preserved in unaltered tektite glass for thousands or millions of years.

Zähringer and Gentner (1963) reported K–Ar ages for tektites from different strew fields. In addition, they report on excess gases from bubble-rich tektites. The measured $^{40}Ar/^{36}Ar$ ratios varied between 296 and 305, which overlaps with the value of modern air of 296.2 (Mark et al. 2011). The gas composition in bubbles of indochinites, moldavites, Libyan desert glass, and glass from the Ries impact site in Nördlingen was further investigated by means of gas chromatography by Müller and Gentner (1968). The discovered O_2 with and observed a N_2/O_2 ratio varied around 4, which is close to the modern atmospheric value of 3.7 (from the volume mixing ratio). The measured N_2/CO_2 ratios for the Muong Nong tektites, which are younger than 1 Ma, vary between 16 and 160 and are much lower than the ratio of ~3000 about 0.7 Ma ago. Jessberger and Gentner (1972) studied the gas composition (N_2, O_2, CO_2, CO, SO_2, Ar, Kr, Xe) in bubbles from the Muong Nong tektites and from Libyan desert glass by means of mass spectrometry. Samples were crushed in vacuum and the released gases were analyzed in a quadrupole mass spectrometer. They reported noble gas isotope ratios resembling that of modern air. The N_2/O_2 ratios all exceeded the atmospheric value by up to a factor of a thousand. Jessberger and Gentner (1972) suggested that O_2 was consumed by an unspecified oxidation process.

To date, the author is not aware of any other isotope data of the O_2 from the inclusions in tektites. Even if the $\delta^{18}O$ would have been modified by mass-dependent fractionation, e.g., thorough preferential uptake of ^{16}O during oxidation processes, the $\Delta'^{17}O$ could still be reconstructed. Also, diffusional loss of gas and contamination by recent air needs to be considered. Small amounts of gas, however, make such measurements an analytical challenge.

Skeletal apatite and eggshell carbonate

The oxidation of carbohydrates, protein, and fat by inhaled O_2 in animals is accompanied by mass transfer from anomalous O_2 into body water. From that body water, skeletal apatite (bones and teeth) and calcite (eggshells) are precipitated and can, in principle, record the triple isotope composition of the respective body fluid (see Kohn 1996). If that animal lived in times of elevated CO_2 concentrations, $\Delta'^{17}O$ of the inhaled O_2 was lower and hence the $\Delta'^{17}O$ of body fluid would have been lower. The $\Delta'^{17}O$ signature is then transferred from the body water into bioapatite and egg shell carbonate, where its being preserved.

This approach has been introduced by Pack et al. (2013) for bioapatite and Passey et al. (2014) for eggshell calcite. A few applications have since been published (Pack et al. 2013; Passey et al. 2014; Gehler et al. 2011, 2014). Details about that approach are summarized by Passey and Levin (2021, this volume).

High temperature technical products

Technical magnesia and alumina. In this section, I will present a few data on technical products that had interacted with atmospheric O_2. Sintered magnesia (periclase, MgO, $T_{melting}$ = 2852 °C) and alumina (corundum, Al_2O_3, $T_{melting}$ = 2072 °C) are common materials for high-*T* applications. Magnesia is produced by thermal decomposition of magnesite ($MgCO_3$) or brucite ($Mg[OH_2]$; e.g., Drnek 2018; Herbrich et al. 1990). The reaction product is so-called caustic magnesia, which is extremely fine-grained and highly reactive. For high-*T* refractories, coarse-grained magnesia is required, which is obtained by sintering or melting of caustic magnesia (Drnek 2018). Magnesia sintering requires temperatures of 1800–2200 °C. Electric arc melting reaches temperatures exceeding 2852°C to melt the magnesia.

Sintering includes destruction and reconstruction of the crystal structure. Such process may allow the exchange of oxygen between the furnace atmosphere (air) and the oxide (alumina, magnesia) refractory. Pure diffusional exchange is a slow process, even at very high temperatures and is not considered here to be important for the exchange of oxygen between the atmosphere and refractories.

Herbrich et al. (1990) studied the isotope composition of magnesia during the decalcination and the sintering in process. They fluorinated magnesia using F_2 gas in conventional Ni reaction vessels. The furnace atmosphere during the Czochralski growth process was oxidizing. They observed that the $\delta^{18}O$ of the magnesia products changes towards the composition of the furnace atmosphere, which was measured to be identical to that of air O_2. The sintered pellets had a higher $\delta^{18}O$ on their outer parts compared the interior, which had $\delta^{18}O \approx 13‰$. A similar observation has been made by Pack et al. (2005), who studied the oxygen isotope composition of a 3.5 cm large sintered magnesia pellet. The magnesia was analyzed by means of laser fluorination with F_2 as oxidant in combination with continuous flow gas source mass spectrometry (Pack 2000; Pack et al. 2005). The $\delta^{18}O$ increased from 8‰ in the interior towards 15‰ at the surface of the pellet. Pack et al. (2005) reported bulk $\delta^{18}O = 14‰$ for three different magnesia raw materials used for steelmaking, which is close to the bulk number of 13‰ reported by Herbrich et al. (1990). Herbrich et al. (1990) present a detailed photography of the sintered magnesia that revealed newly formed cubes of periclase. The isotope composition of this magnesia as measured to $\delta^{18}O = 22‰$, i.e., very close to the composition of air O_2. The idiomorphic crystals of magnesia either formed by sublimation and re-sublimation of MgO or by localized magnesia reduction and re-precipitation by oxidation with O_2 from the furnace atmosphere (Herbrich et al. 1990). Herbrich et al. (1990) favor the reduction in combination with evaporation and oxidation in combination with re-sublimation pathway and suggest that carbon is the reducing agent. The difference of 1.9‰ between air O_2 and magnesia could reflect the high-*T* equilibrium between magnesia and O_2. High-*T* equilibrium fractionation of the same order (–2.5‰) has been observed for the silicate melt O_2 equilibrium (Fig. 6).

No triple oxygen isotope data have been published of technical magnesia. It is expected that the newly-formed magnesia described by Herbrich et al. (1990) has a $\Delta'^{17}O$ that is about 0.004‰ lower than that of air O_2, i.e., –0.435‰. This estimate is based on a θ of 0.53 for the magnesia-O_2 high-*T* equilibrium.

As in the case of magnesia, sintering of alumina may also have an effect on its triple oxygen isotope composition. The bauxite raw materials have $\delta^{18}O$ values in the range of 6–13‰ (Bird et al. 1989, 1993; Ellahi et al. 2016) expected to fall in the $\Delta'^{17}O$ field typical for low-*T* rocks and minerals. The Bayer process (Habashi 1995) includes dissolution of bauxite and precipitation as $Al(OH)_3$, which may lead to mass-dependent fractionation due to exchange with the solvent. Alumina is then produced from the hydroxide by dehydration at 1200–1300 °C, a step that likely also includes mass-dependent fractionation effects and, possibly, already some exchange with the atmosphere. The major exchange step, however, would be the sintering, which is done at >1600 °C. For two alumina materials used as refractory in steelmaking Pack et al. (2005), determined 18‰ ≤ $\delta^{18}O$ ≤ 20‰.

So far, no triple oxygen isotope analyses have been published on high-*T* refractories. A PostDoc from my group, Dr. Nina Albrecht, conducted first triple oxygen isotope measurements on technical alumina (Table 2). The material was a densely sintered alumina crucible for application in high-*T* furnace experiments. She obtained a $\delta^{18}O$ of 16.5‰ and a $\Delta'^{17}O$ as low as –0.270‰ (Fig. 7).

The $\delta^{18}O$ of the sintered alumina is close to the data reported by Pack et al. (2005) for alumina refractories. The $\Delta'^{17}O$ of the sintered alumina is clearly much lower than what has been measured for natural rocks and minerals (Fig. 7). A simple mass balance indicates ~60% exchange with atmospheric O_2 during sintering (Fig. 7). For comparison, Dr. Albrecht analyzed a set of natural corundum, ruby, and sapphire samples (Table 2). They range in $\delta^{18}O$ from 12 to 26‰, but have $\Delta'^{17}O$ values typical of sediments (Fig. 7). For comparison, Giuliani et al. (2005) reported similarly spreading $\delta^{18}O$ values of 3 to 23‰ from various ruby and sapphire deposits.

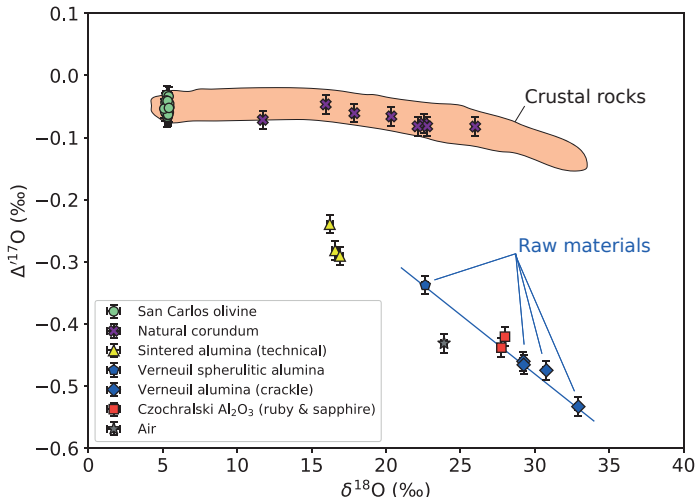

Figure 7. Plot of $\Delta'^{17}O$ vs. $\delta^{18}O$ of natural (**purple filled crosses**, corundum, ruby sapphire) and sintered technical (**yellow filled triangles**) alumina. The range of typical terrestrial crustal rocks and data for San Carlos olivine (**light green filled circles**) and air O_2 (**gray filled star**) are displayed (e.g., Pack and Herwartz 2014; Bindeman et al. 2018, 2019; Bindeman 2021, this volume). Data for synthetic corundum starting materials (**pentagon, diamonds**), and Czochralski grown ruby and sapphire crystal (**red filled square**) are displayed. The corresponding data are listed in Table 2.

Table 2. List with description and oxygen isotope data for the analyzed corundum samples. The materials were provided by Dr. Klaus Dupré of the Forschungsinstitut für Mineralogische und Metallische Werkstoffe Edelmetalle/Edelsteine (FEE) in Idar Oberstein and by Dr. Alexander Gehler from the collection of the Geoscience Center in Göttingen (GZG). The $\Delta'^{17}O$ is reported relative to a slope = 0.528 reference line.

Sample	Comment	Source	$\delta^{17}O$	$\delta^{18}O$	$\Delta'^{17}O$
Sapphire (Ceylon)	Sri Lanka	GZG Collection	9.336	17.873	–0.082
Ruby (Ceylon)	Sri Lanka	GZG Collection	13.558	25.993	–0.066
– “” –	– “” –	– “” –	10.633	20.361	–0.082
– “” –	– “” –	– “” –	11.534	22.116	–0.061
Ruby (Slatoust)	Ural, Russia	GZG Collection	11.874	22.767	–0.082
Technical alumina	Commercial	Laboratory	8.44	16.58	–0.281
– “” –	– “” –	– “” –	8.29	16.22	–0.239
Alumina microbeads	~ 50 µm spherulitic powder, oxyhydrogen flame fused	FEE Idar Oberstein	11.548	22.637	–0.338
Crackle corundum	Coarse fraction, Verneuil	FEE Idar Oberstein	14.865	29.237	–0.460
– “” –	Fine fraction, Verneuil	FEE Idar Oberstein	14.866	29.25	–0.466
– “” –	– “” –	FEE Idar Oberstein	15.652	30.777	–0.475
– “” –	– “” –	FEE Idar Oberstein	16.71	32.925	–0.533
Sapphire FEE	Czochralski XX	FEE Idar Oberstein	14.258	27.995	–0.420
Ruby FEE	Czochralski XX	FEE Idar Oberstein	14.115	27.754	–0.438
San Carlos olivine	$N = 20$ (av.)	Arizona, USA	2.745	5.306	–0.052

The $\delta^{18}O$ of magnesia refractories and first $\delta^{17}O$ and $\delta^{18}O$ data for technical alumina clearly show that during the high-T production processing of these materials, considerable exchange occurs between the atmosphere and the refractory product. The studied alumina refractory carries a triple oxygen isotope signature that suggests ~ 60% equilibration with the atmosphere.

Using $\Delta'^{17}O$ as a new tool to distinguish synthetic and natural gems

The most common technique of producing single crystals of alumina is growing them by continuously pulling the growing crystal out of a melt (Czochralski 1918). After his inventor, this technique is now called the Czochralski method (see Tomaszewski 2002, for some dispute on the name). An illustration of the process is given in (Fig. 8A). Earlier, Verneuil (1904) described a method for the production of single crystals of corundum, ruby or sapphire; a method now named after him as Verneuil process (Smith 1908). In that process, fine alumina powder is rinsed through an oxyhydrogen torch, in which the powder melts and coagulates to fine alumina droplets (Fig. 8B). The droplets of liquid alumina then fall onto a seed crystal, where they grow to form a single crystal of corundum, ruby, or sapphire. For high-quality and larger crystals, this technique is inferior compared to the Czochralski method. It is, however, used for the preparation of starting materials used in the Czochralski process.

We have obtained three natural ruby and sapphire samples and five samples of synthetic corundum (Table 2).

Sample “Alumina microbeads” consists of a granulate of ~50 µm large alumina spherules. No details about the production process are available. The alumina spherules were likely produced by oxyhydrogen flame fusion in an apparatus similar to that invented by Verneuil (1904), except that the molten droplets were not grown on a single crystal but quenched and

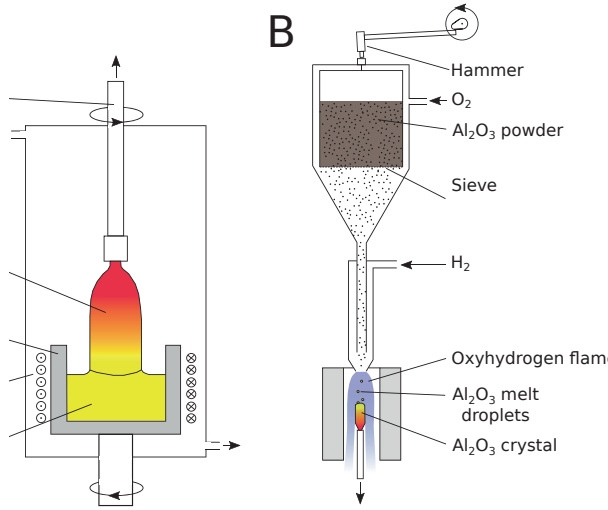

Figure 8. Sketches illustrating the Czochralski method (**A**) and the Verneuil method (**B**, modified after Blumberg and Müller 1970). In the Czochralski method (A) a crystal is grown by continuously pulling out of an alumina melt. In the Verneuil process (B), alumina powder is melted to small droplets that fall onto the growing crystal, where they crystallize in the same lattice orientation as the underlying crystal substrate.

collected as small spherules. Data about the composition of the alumina starting material as well as about the oxygen isotope composition of the O_2 used, however, are not known. The second sample is "Crackle corundum", which is a granulate made by crushing of alumina crystals that were produced by the Verneuil process. As in the case of "Alumina microbeads", not further details about the production process, e.g., the composition of the O_2 gas used, are known. A mixture of "Alumina microbeads" and "Crackle" corundum was used as starting material for the Czochralski process. The pre-fused material is used because of its higher bulk density. Usage of powdered alumina from the Bayer process would require fusion, followed by refilling of the crucible before the growth can start.

A Czochralski-grown ruby and a Czochralski-pulled sapphire (both FEE, Idar-Oberstein, Table 2) were also analyzed. The ruby and sapphire were pulled from an alumina melt at a temperature exceeding the melting point of alumina at 2072°C. The atmosphere during the crystal growth was a mixture of N_2 with 0.5 vol.% of air, i.e., 0.105 vol.% O_2. The melt mass was 6–8 kg and the crystal pulling took ~ 10 days. The apparatus was flushed at a rate of 0.5 $m^3\ h^{-1}$. This translates to a total amount of oxygen of 10.3 mol O (in form of O_2) that went through the apparatus. This number is small compared to the 208 mol O that is contained in 7 kg of well-mixed liquid alumina. This small mass balance calculation demonstrates that, under given growth conditions, as maximum, only 5% of the alumina can have equilibrated with air. In reality, this number may well be an order of magnitude lower as only a small fraction of the O_2 contained in the N_2 atmosphere ever will have touched the melt surface.

The oxygen isotope compositions of the oxyhydrogen flame fused and the Verneuil alumina starting materials and the Czochralski grown ruby and sapphire are listed in Table 2 and illustrated in Fig. 7. The $\delta^{18}O$ of the oxyhydrogen flame fused and Verneuil starting material ("Alumina microbeads" and "Crackle") varies from 22 to 33‰. The variations among the different fragments of the "Crackle" (Table 2) are attributed to the rapid and likely incomplete exchange process between the alumina melt droplets and flame oxygen while the droplets fall through the flame. The data fall on a tight mixing trend of the raw materials with slope $\lambda = 0.509$.

Although air O_2 does not fall on that trend, the low $\Delta'^{17}O$ of the raw materials and the crystals made from them is clearly related to the influence technical O_2 that was prepared by liquefaction from air O_2. Pack et al. (2007) showed that technical O_2 can vary in $\delta^{18}O$ between 0 and 30‰, but, because of mass-dependent fractionation during the oxygen production ($\lambda \approx 0.524$), that the anomaly in $\Delta'^{17}O$ is preserved.

The isotope compositions of the Czochralski grown ruby and sapphire plot on a mixing trend between "Alumina microbeads" and "Crackle" (Fig. 7), which is expected as these materials were used as starting materials. It was discussed that likely no isotope exchange had affected the isotope composition of the melt during the Czochralski process. The observation that the $\Delta'^{17}O$ of the sapphire and ruby crystals is identical to that of air is a mere coincidence and results from the compositions and mixing ratios of the raw materials.

The data presented here show that synthetic alumina (corundum, ruby, sapphire) can clearly be distinguished from natural corundum, ruby and sapphire in that the synthetic crystals have a much lower $\Delta'^{17}O$ resembling that of air O_2 and its technical derivatives. Hence, $\Delta'^{17}O$ is a clear and difficult-to-manipulate indicator of the gemstone formation process. The studied Czochralski grown ruby and sapphire crystals largely reflect the $\Delta'^{17}O$ of the modern atmosphere along with mass-dependent variation due to the liquefaction process. As such, they can be regarded a suitable proxy for the $p_{CO_2} \cdot GPP$. One can imagine that a centimeter to decimeter sized synthetic alumina crystal is highly resistant to any kind of isotopic modification by geological processes. In the far future (e.g., billions of years from now), such then fossil Czochralski-grown ruby and sapphire crystals buried in sedimentary rocks could serve an isotope geochemist as a unique tracer of anthropogenic activity and as an atmospheric proxy.

CONCLUSIONS

It has been stated by Bao (2015) "[…] that sulfate, to this point, is the only compound from which direct atmospheric O_2 and O_3 signals from the distant past can be retrieved." In this chapter, I highlight that not only sulfate, but a number of other solids carry information about the isotope anomaly of air O_2. The processes are exchange at high temperatures and/or transfer of O_2 during an oxidation process. Some of the materials are potential proxies for the $\Delta'^{17}O$ of air O_2.

ACKNOWLEDGEMENTS

The constructive reviews by Laurence Y. Yeung and Huimin Bao helped improving the manuscript. Ilya Bindeman is thanked for initiating this volume, his comments and for the editorial handling. Dennis Kohl, Nina Albrecht, and the entire lab team is thanked for their various contributions. Klaus Dupré is thanked for providing alumina crystals ad background information. Christian Stübler is thanks for allowing me to use his data from his BSc theses.

REFERENCES

Affolter S, Häuselmann AD, Fleitmann D, Häuselmann P, Leuenberger M (2015) Triple isotope (δD, $\delta^{17}O$, $\delta^{18}O$) study on precipitation, drip water and speleothem fluid inclusions for a Western Central European cave (NWSwitzerland). Quat Sci Rev 127:73–89

Ash JL, Hu H, Yeung LY (2020) What fractionates oxygen isotopes during respiration? insights from multiple isotopologue measurements and theory. ACS Earth Space Chem 4:50–66

Balci N, Shanks IIIW C, Mayer B, Mandernack KW (2007) Oxygen and sulfur isotope systematics of sulfate produced by bacterial and abiotic oxidation of pyrite. Geochim Cosmochim Acta 71:3796–3811

Bao H (2015) Sulfate: A time capsule for Earths O_2, O_3, and H_2O. Chem Geol 395:108–118

Bao H, Lyons J, Zhou C (2008) Triple oxygen isotope evidence for elevated CO_2 levels after a Neoproterozoic glaciation. Nature 54:349–392
Bao H, Cao X, Hayles JA (2016) Triple oxygen isotopes: fundamental relationships and applications. Ann Rev Earth Planet Sci 44:463–492
Barkan E, Luz B (2003) High-precision measurements of $^{17}O/^{16}O$ and $^{18}O/^{16}O$ of O_2 and O_2/Ar ratio of air. Rapid Commun Mass Spectrom 17:2809–2814
Barkan E, Luz B (2005) High precision measurements of $^{17}O/^{16}O$ and $^{18}O/^{16}O$ ratios in H_2O. Rapid Commun Mass Spectrom 19:3737–3742
Barkan E, Luz B (2011) The relationships among the three stable isotopes of oxygen in air, seawater and marine photosynthesis. Rapid Commun Mass Spectrom 25:2367–2369
Bender M, Sowers T, Labeyrie L (1994) The Dole effect and its variations during the last 130,000 years as measured in the Vostok ice core. Global Biogeochem Cycles 8:363–376
Benson BB, Krause Jr D (1984) The concentration and isotopic fractionation of oxygen dissolved in freshwater and seawater in equilibrium with the atmosphere. Limnol Oceanogr 29, 620–632
Bindeman IN (2021) Triple oxygen isotopes in evolving continental crust, granites, and clastic sediments. Rev Mineral Geochem 86:241–290
Bindeman I, Zakharov D, Palandri J, Greber ND, Dauphas N, Retallack G, Hofmann A, Lackey J, Bekker A (2018) Rapid emergence of subaerial landmasses and onset of a modern hydrologic cycle 2.5 billion years ago. Nature 557:545–548
Bindeman IN, Bayon G, Palandri J (2019) Triple oxygen isotope investigation of fine-grained sediments from major world's rivers: Insights into weathering processes and global fluxes into the hydrosphere. Earth Planet Sci Lett 528:115851
Bird MI, Chivas AR, Andrew AS (1989) A stable-isotope study of lateritic bauxites. Geochim Cosmochim Acta 53:1411–1420
Bird MI, Longstaffe FJ, Fyfe WS, Kronberg BI, Kishilda A (1993) An oxygen-isotope study of weathering in the eastern Amazon Basin, Brazil. Washington DC. American Geophysical Union Geophysical Monograph Series 78:295–307
Blumberg H, Müller R (1970) Automatische Verneuil—Apparatur zur Züchtung von Rubin-Einkristallstäben. Kristall und Technik 5:33–36
Blunier T, Barnett B, Bender ML, Hendricks MB (2002) Biological oxygen productivity during the last 60,000 years from triple oxygen isotope measurements. Global Biogeochem Cycles 16:1029
Blunier T, Bender M, Barnett B, von Fischer J (2012) Planetary fertility during the past 400 ka based on the triple isotope composition of O_2 in trapped gases from the Vostok ice core, Climate of the Past 8:1509–1526
Bouška V, Povondra P, Florenskij P, Řanda Z (1981) Irghizites and zhamanshinites: Zhamanshin crater, USSR. Meteoritics 16:171–184
Buchwald VF (1977) Mineralogy of iron meteorites. Phil Trans R Soc London Ser A 286:453–491
Cao X, Bao H (2013). Dynamic model constraints on oxygen-17 depletion in atmospheric O_2 after a snowball Earth. PNAS 110:14546–14550
Cao X, Bao H (2021) Small triple oxygen isotope variations in sulfate: Mechanisms and applications. Rev Mineral Geochem 86: 463–488
Catling DC, Zahnle KJ (2020) The Archean atmosphere. Sci Adv 6:1420
Clayton RN, Mayeda TK (1996) Oxygen isotope studies of achondrites. Geochim Cosmochim Acta 39:569–584
Clayton RN, Mayeda TK, Brownlee DE (1986) Oxygen isotopes in deep-sea spherules. Earth Planet Sci Lett 79:235–240
Crockford PW, Hayles JA, Bao H, Planavsky NJ, Bekker A, Fralick PW, Halverson GP, Bui TH, Peng Y, Wing BA (2018) Triple oxygen isotope evidence for limited mid-Proterozoic primary productivity. Nature 559:613–616
Czochralski J (1918) Ein neues Verfahren zur Messung der Kristallisationsgeschwindigkeit der Metalle. Z für Physikalische Chemie 92:219–221
Davis AM, Brownlee DE (1993) Iron and nickel isotopic mass fractionation in deep-sea spherules. XXIV Lunar and Planetary Science Conference (Houston) p. 373–374
Davis AM, Clayton RN, Mayeda TK, Brownlee DE (1991) Large mass fractionation of iron isotopes in cosmic spherules collected from deep-sea sediments. XXII. Lunar and Planetary Science Conference (Houston) p. 281–282
Dole M (1936) The relative atomic weight of oxygen in water and in air. J Chem Phys 4:268–275
Dole M, Lane GA, Rudd DP, Zaukelies DA (1954) Isotopic composition of atmospheric oxygen and nitrogen. Geochim Cosmochim Acta 6:65–78
Donaldson CH, Williams RJ, Lofgren G (1975) A sample holding technique for study of crystal growth in silicate melts. Am Mineral 60:324–326
Drnek T (2018) Magnesit im Überblick. res montanarum. Z des Montanhistorischen Vereins für Österreich 58:5–12
Ellahi SS, Taghipour B, Zarasvandi A, Bird MI, Somarin AK (2016) Mineralogy, geochemistry and stable isotope studies of the Dopolan Bauxite Deposit, Zagros Mountain, Iran. Minerals 6:1–21
Engrand C, McKeegan KD, Leshin LA, Herzog GF, Schnabel C, Nyquist LE, Brownlee DE (2005) Isotopic compositions of oxygen, iron, chromium, and nickel in cosmic spherules: Toward a better comprehension of atmospheric entry heating effects. Geochim Cosmochim Acta 39:569–584
Farquhar J, Bao H, Thiemens M (2000) Atmospheric influence of Earths earliest sulfur cycle. Science 339:780–785
Florenski PV (1977) Der Meteoritenkrater Zhamanshin (nördliches Aralgebiet, UdSSR) und seine Tektite und Impaktite. Chemie der Erde 36:83–95

Gehler A, Tütken T, Pack A (2011) Triple oxygen isotope analysis of bioapatite as tracer for diagenetic alteration of bones and teeth, Palaeogeogr Palaeoclimatol Palaeoecol 310:84–91
Gehler A, Gingerich PD, Pack A (2016) Temperature and atmospheric CO_2 concentration estimates through the PETM using triple oxygenisotope analysis of mammalian bioapatite, PNAS 113:7739–7744
Genge MJ, Engrand C, Gounelle M, Taylor S (2008) The classification of micrometeorites. Meteorit Planet Sci 35:807–816
Genge MJ (2016) The origins of I-type spherules and the atmospheric entry of iron micrometeoroids. Meteorit Planet Sci 51:1–19
Giauque WF, Johnston HL (1929) An isotope of oxygen of mass 17 in the Earth's atmosphere, Nature 54:349–392
Giuliani G, Fallick AE, Garnier V, France-Lanord C, Ohnenstetter D, Schwarz D (2005) Oxygen isotope composition as a tracer for the origins of rubies and sapphires. Geology 33:249–252
Graham T (1863) On the molecular mobility of gases. Philos Trans R Soc 153:385–405
Graham RJ, Shaw TA, Abbot DS (2019). The Snowball Stratosphere. J Geophys Res: Atmospheres 124:11819–11836
Habashi F (1995) Bayers process for alumina production: a historical perspective. Bull History Chem 17/18:15–19
Heinzinger K, Iunge C, Schidlowski M (1971) Oxygen isotope ratios in the crust of iron meteorites. Z Naturforsch 26:1485–1490
Hendricks MB, Bender ML, Barnett BA, Strutton P, Chavez FP (2005) Triple oxygen isotope composition of dissolved O_2 in the equatorial Pacific: A tracer of mixing, production, and respiration, J Geophys Res: Oceans 110: C12
Herbrich P, Mörtl G, Hoernes S (1990) Der Anteil von schwerem Sauerstoff (^{18}O) in Sintermagnesia-Produkten. Radex-Rundschau 1990:275–283
Jessberger E, Gentner W (1972) Mass spectrometric analysis of gas inclusions in Muong Nong glass and Libyan Desert glass. Earth Planet Sci Lett 14:221–225
Koeberl C (1988) The origin of tektites: a geochemical discussion. Proceedings of the National Institute of Polar Research Symposium on Antarctic Meteorites 1:261–290
Koeberl C (1994) Tektite origin by hypervelocity asteroidal or cometary impact. Large meteorite impacts and planetary evolution 293:133–151
Koeberl C, Fredriksson K (1986) Impact glasses from Zhamanshin crater (USSR): chemical composition and discussion of origin. Earth Planet Sci Lett 78:80–88
Kohl I, Bao H (2011). Triple-oxygen-isotope determination of molecular oxygen incorporation in sulfate produced during abiotic pyrite oxidation (pH= 2–11). Geochim Cosmochim Acta, 75:1785–1798
Kohn MJ (1996) Predicting animal $\delta^{18}O$: accounting for diet and physiological adaption, Geochim Cosmochim Acta 39:569-584
Krinov E, Brown H, Anders E (1961) Principles of Meteoritics. Pergamon (London), 552 pp
Kroopnick P, Craig H (1972) Atmospheric oxygen: isotopic composition and solubility fractionation. Science 175:54–55
Kroopnick P, Craig H (1976) Oxygen isotope fractionation in dissolved oxygen in the deep sea. Earth Planet Sci Lett 32:375–388
Landais A, Barkan E, Luz B (2008) Record of $\delta^{18}O$ and $^{17}O_{excess}$ in ice from Vostok Antarctica during the last 150,000 years. Geophys Res Lett 35:L02709
Laughlin DE, Hono K (Eds.) (2015) Physical Metallurgy. Elsevier (Amsterdam), 2960 pp
Leblanc T, Walsh T, McDermid I, Toon G, Blavier J-F, Haines B, Read W, Herman B, Fetzer E, Sander S, Pongetti T, Whiteman D, McGee T, Twigg L, Sumnicht G, Venable D, Calhoun M, Dirisu A, Hurst D, Hauchecorne A (2011) Measurements of Humidity in the Atmosphere and Validation Experiments (MOHAVE)-2009: overview of campaign operations and results. Atmos Meas Tech Discuss 4:3277–3336
Li S, Levin NE, Chesson LA (2015) Continental scale variation in $^{17}O_{excess}$ of meteoric waters in the United States. Geochim Cosmochim Acta 164:110–126
Li S, Levin NE, Soderberg K, Dennis KJ, Caylor KK (2017) Triple oxygen isotope composition of leaf waters in Mpala, central Kenya. Earth Planet Sci Lett 468:38–50
Li B, Yeung LY, Hu H, Ash JL (2019) Kinetic and equilibrium fractionation of O_2 isotopologues during air-water gas transfer and implications for tracing oxygen cycling in the ocean. Mar Chem 210:61–71
Luo G, Ono S, Beukes NJ, Wang DT, Xie S, Summons RE (2016) Rapid oxygenation of Earth's atmosphere 2.33 billion years ago, Sci Adv 2: e1600134
Luz B, Barkan E, Bender ML, Thiemens MH, Boering KA (1999) Triple-isotope composition of atmospheric oxygen as a tracer of biosphere productivity. Nature 54:349–392
Luz B, Barkan E (2009) Net and gross oxygen production from O_2/Ar, $^{17}O/^{16}O$ and $^{18}O/^{16}O$ ratios. Aquatic Microbial Ecol 56:133–145
Luz B, Barkan E (2010) Variations of $^{17}O/^{16}O$ and $^{18}O/^{16}O$in meteoric waters. Geochim Cosmochim Acta 74:6276–6286
Luz B, Barkan E (2011) Oxygen isotope fractionation in the ocean surface and $^{18}O/^{16}O$ of atmospheric O_2. Global Biogeochem Cycles 25: GB4006
Luz B, Barkan E, Severinghaus JP, (2014) The stable isotopic composition of atmospheric O_2. *In:* Holland HD, Turekian KK (Eds.) Treatise in Geochemistry Elsevier (Amsterdam), p. 363–383

Magna T, Žák K, Pack A, Moynier F, Mougel B, Skála R, Jonášová S, Řanda Z, Mizera J (2017) Zhamanshin astrobleme provides evidence for carbonaceous chondrite and post-impact exchange between ejecta and Earth's atmosphere. Nat Commun 8:227

Mandernack KW, Fogel ML, Tebo BM, Usui A (1995) Oxygen isotope analyses of chemically and microbially produced manganese oxides and manganates. Geochim Cosmochim Acta 59:4409–4425

Macris CA, Asimow PD, Badro J, Eiler JM, Zhang Y, Stolper EM (2018) Seconds after impact: Insights into the thermal history of impact ejecta from diffusion between lechatelierite and host glass in tektites and experiments, Geochim Cosmochim Acta 241:69–94

Mark D, Stuart F, De Podesta M (2011) New high-precision measurements of the isotopic composition of atmospheric argon. Geochim Cosmochim Acta 75:7494–7501

Matsuhisa Y, Goldsmith JR, Clayton RN (1978) Mechanisms of hydrothermal crystallization of quartz at 250°C and 15 kbar. Geochim Cosmochim Acta 42:173–182

McKinney CR, McCrea JM, Epstein S, Allen HA, Urey HC (1950) Improvements in mass spectrometers for the measurement of small differences in isotope abundance ratios. Rev Sci Instrum 21:724–730

Miller MF, Pack A (2021) Why Measure ^{17}O? Historical perspective, triple-isotope systematics and selected applications. Rev Mineral Geochemistry 86:1–34

Mizera J, Řanda Z, Tomandl I (2012) Geochemical characterization of impact glasses from the Zhamanshin crater by various modes of activation analysis. Remarks on genesis of irghizites. J Radioanal Nucl Chem 293:359–376

Müller O, Gentner W (1968) Gas content in bubbles of tektites and other natural glasses. Earth Planet Sci Lett 4:406–410

Nicholson D, Stanley RH, Doney SC (2014) The triple oxygen isotope tracer of primary productivity in a dynamic ocean model, Global Biogeochem Cycles 28:538–552

Pack A (2000) Tracing the origin of oxide inclusions in continuously casted steel. PhD thesis, Rheinische Friedrich Wilhelms Universität, Bonn, 164 pp

Pack A, Herwartz D (2014) The triple oxygen isotope composition of the Earth mantle and understanding $\Delta^{17}O$ variations in terrestrial rocks and minerals. Earth Planet Sci Lett 390:138–145

Pack A, Hoernes S, Göbbels M, Broß R, Buhr A (2005) Stable oxygen isotopes—a new approach for tracing the origin of oxide inclusions in steel. Euro J Mineral 17:483–493

Pack A, Toulouse C, Przybilla R (2007) Determination of oxygen triple isotope ratios of silicates without cryogenic separation of NF_3—technique with application to analyses of technical O_2 gas and meteorite classification. Rapid Commun Mass Spectrom 21:3721–3728

Pack A, Gehler A, Süssenberger A (2013) Exploring the usability of isotopically anomalous oxygen in bones and teeth as paleo-CO_2-barometer, Geochim Cosmochim Acta 102: 306–317

Pack A, Tanaka R, Hering M, Sengupta S, Peters S, Nakamura E (2016) The oxygen isotope composition of San Carlos olivine on VSMOW2-SLAP2 scale. Rapid Commun Mass Spectrom 30:1495–1504

Pack A, Höweling A, Hezel DC, Stefanak M, Beck AK, Peters ST M, Sengupta S, Herwartz D, Folco L (2017) Tracing the oxygen isotope composition of the upper Earth atmosphere using cosmic spherules. Nat Commun 8:15702

Payne RC, Brownlee D, Kasting JF (2020) Oxidized micrometeorites suggest either high pCO_2 or low pN_2 during the Neoarchean, PNAS 117:1360

Passey BH, Levin NE (2021) Triple oxygen isotopes in meteoric waters, carbonates, and biological apatites: implications for continental paleoclimate reconstruction. Rev Mineral Geochemistry 86:429–462

Peters ST, Alibabaie N, Pack A, McKibbin SJ, Raeisi D, Nayebi N, Torab F, Ireland T, Lehmann B (2020) Triple oxygen isotope variations in magnetite from iron-oxide deposits, central Iran, record magmatic fluid interaction with evaporite and carbonate host rocks. Geology 48:211–215

Sengupta S, Pack A (2018) Triple oxygen isotope mass balance for the Earth's oceans with application to Archean cherts. Chem Geol 495:18–26

Sharp ZD, Wostbrock J (2021) Standardization for the triple oxygen isotope system: Waters, silicates, carbonates, air, and sulfates. Rev Mineral Geochem 86: 179–196

Sharp ZD, Gibbons JA, Atudorei V, Pack A, Sengupta S, Shock EL, Knauth LP (2016) A calibration of the triple oxygen isotope fractionation in the SiO_2–H_2O system and applications to natural samples. Geochim Cosmochim Acta 186:105–119

Sharp Z, Wostbrock J, Pack A (2018) Mass-dependent triple oxygen isotope variations in terrestrial materials. Geochem Perspect Lett 7:27–31

Shuvalov V, Dypvik H (2013) Distribution of ejecta from small impact craters. Meteorit Planet Sci 48:1034–1042

Silverman SR (1951) The isotope geology of oxygen. Geochim Cosmochim Acta 39:569–584

Smith GH (1908) Note on synthetical corundum and spinel. Mineral Mag 15:153–155

Spencer LJ (1933) Origin of tektites. Nature 131:117–118

Stolper DA, Fischer WW, Bender ML (2018) Effects of temperature and carbon source on the isotopic fractionations associated with O_2 respiration for $^{17}O/^{16}O$ and $^{18}O/^{16}O$ ratios in *E coli*, Geochim Cosmochim Acta 240:152–172

Stübler C (2017) Hochtemperaturaustausch von Sauerstoffisotopen zwischen Silikatschmelzen und der Atmosphäre, Georg-August-Universität, Göttingen, 55 pp

Surma J, Assonov S, Bolourchi M, Staubwasser M (2015) Triple oxygen isotope signatures in evaporated water bodies from the Sistan Oasis, Iran. Geophys Res Lett 42:8456–8462

Surma J, Assonov S, Herwartz D, Voigt C, Staubwasser M (2018) The evolution of $^{17}O_{excess}$ in surface water of the arid environment during recharge and evaporation. Sci Rep 8:1–10
Sutherland KM, Wostbrock JA, Hansel CM, Sharp ZD, Hein JR, Wankel SD (2020) Ferromanganese crusts as recorders of marine dissolved oxygen. Earth Planet Sci Lett 533:116057
Taylor HP, Epstein S (1962) Oxygen isotope studies on the origin of tektites. J Geophys Res 67:4485–4490
Tappert R, McKellar RC, Wolfe AP, Tappert MC, Ortega-Blanco J, Muehlenbachs K (2013) Stable carbon isotopes of C3 plant resins and ambers record changes in atmospheric oxygen since the Triassic. Geochim Cosmochim Acta 121:240–262
Thiemens MH, Meagher D (1984) Cryogenic separation of nitrogen and oxygen in air for determination of isotopic ratios by mass spectrometry. Anal Chem 56:201–203
Thiemens MH, Jackson T, Zipf EC, Erdman PW, van Egmond C (1995) Carbon dioxide and oxygen isotope anomalies in the mesosphere and stratosphere. Science 339:780–785
Tian C, Wang L (2019) Stable isotope variations of daily precipitation from 2014–2018. Scientific Data 6:190018
Tian C, Wang L, Kaseke KF, Bird BW (2018) Stable isotope compositions (δ^2H, $\delta^{18}O$ and $\delta^{17}O$) of rainfall and snowfall in the central United States. Sci Rep 8:1–15
Tomaszewski PE (2002) Jan Czochralski–father of the Czochralski method. J Cryst Growth 236:1–4
Tomkins AG, Bowlt L, Genge M, Wilson SW, Brand HE A, Wykes JL (2016) Ancient micrometeorites suggestive of an oxygen-rich Archaean upper atmosphere. Nature 533:235–238
Touzeau A, Landais A, Stenni B, Uemura R, Fukui K, Fujita S, Guilbaud S, Ekaykin A, Casado M, Barkan E (2016) Acquisition of isotopic composition for surface snow in East Antarctica and the links to climatic parameters. The Cryosphere 10:837–852
Urey HC (1955) On the origin of tektites. PNAS 41:27–31
Verneuil AV L (1904) Mémoires sur la reproduction artificielle du rubis par fusion. Annales de Chimie et de Physique Sér. 8, Vol. III: 20–45
Wang J, Davis AM, Clayton RN, Mayeda TK (1994) Kinetic Isotopic Fractionation During the Evaporation of the Iron Oxide from Liquid State. XXV Lunar and Planetary Science Conference (Houston) abstract #1459
Winter J (2001) An introduction to igneous and metamorphic petrology. Prentice-Hall (Upper Saddle River, NJ), 697 pp
Wostbrock JA, Cano EJ, Sharp ZD (2020) An internally consistent triple oxygen isotope calibration of standards for silicates, carbonates and air relative to VSMOW2 and SLAP2. Chem Geol 533:119432
Yeung LY, Young ED, Schauble EA (2012) Measurements of $^{18}O^{18}O$ and $^{17}O^{18}O$ in the atmosphere and the role of isotope-exchange reactions, J Geophys Res (Atmospheres) 117:18306
Yeung LY, Hayles JA, Hu H, Ash JL, Sun T (2018) Scale distortion from pressure baselines as a source of inaccuracy in tripleâ. Rapid Commun Mass Spectrom 32:1811–1821
Young ED, Galy A, Nagahara H (2002) Kinetic and equilibrium mass-dependent isotope fractionation laws in nature and their geochemical and cosmochemical significance. Geochim Cosmochim Acta 66:1095–1104
Young ED, Yeung LY, Kohl IE (2014) On the $\Delta^{17}O$ budget of atmospheric O_2. Geochim Cosmochim Acta 135:102–125
Zähringer J, Gentner W (1963) Radiogenic and atmospheric argon content of tektites. Nature 199:583–583
Zák K, Skála R, Pack A, Ackerman L, Křížová S (2019) Triple oxygen isotope composition of Australasian tektites. Meteorit Planet Sci 54:1167–1181fs